AGU PUBLICATIONS

JGR

Journal of Geophysical Research: Earth Surface

RESEARCH ARTICLE
10.1002/2014JF003148

Key Points:
- Front positions and ice speeds of 28 calving glaciers were studied in the SPI
- The calving glaciers generally retreated and decelerated in 1984–2011
- Three rapidly retreating glaciers accelerated twofold

Supporting Information:
- Readme
- Figure S1
- Figure S2

Correspondence to:
D. Sakakibara,
sakakibara@pop.lowtem.hokudai.ac.jp

Citation:
Sakakibara, D., and S. Sugiyama (2014), Ice-front variations and speed changes of calving glaciers in the Southern Patagonia Icefield from 1984 to 2011, *J. Geophys. Res. Earth Surf.*, *119*, doi:10.1002/2014JF003148.

Received 17 MAR 2014
Accepted 26 OCT 2014
Accepted article online 30 OCT 2014

Ice-front variations and speed changes of calving glaciers in the Southern Patagonia Icefield from 1984 to 2011

Daiki Sakakibara[1,2] and Shin Sugiyama[2]

[1]Graduate School of Environmental Science, Hokkaido University, Sapporo, Japan, [2]Institute of Low Temperature Science, Hokkaido University, Sapporo, Japan

Abstract Patagonian icefields are losing volume, and their loss is due partly to rapid changes in their outlet glaciers that terminate in lakes or the ocean. Despite this key influence from outlet glaciers, relatively few of these calving glaciers have had high-frequency measurements on their frontal variations and ice speed changes. We describe here recent frontal variations and ice speed changes of all 28 major calving glaciers in the Southern Patagonia Icefield (SPI), including ice speed maps covering approximately half of the entire icefield. The analysis is based on satellite data from 1984 to 2011. Over this period, only the two termini of Glaciar Pío XI advanced. Of the remaining glacial fronts, 12 changed less than ±0.5 km, but 17 retreated at least 0.5 km. In the latter group, three glacial fronts (Glaciar Jorge Montt, HPS12, and Upsala) retreated over 6 km. Averaged over all 31 glacial fronts of the calving glaciers, the front positions retreated 1.56 km (median is 0.71 km). Along the flowline within 20 km of the front, the ice speeds up to 5900 ± 200 m a^{-1}. Except for regions showing large acceleration or deceleration, the mean speed over the measured area decreased by 30 m a^{-1} from 1984 to 2011. The three most rapidly retreating glaciers showed much larger acceleration near the calving front, suggesting that ice dynamics drive their rapid retreat. Thus, we see retreat as a long-term trend for the calving glaciers in the SPI, with behavior that implies a dynamically controlled rapid recession that may explain the recently reported volume change of the SPI.

1. Introduction

The Northern and Southern Patagonia Icefields (NPI and SPI) cover areas of 3950 [*Rivera et al.*, 2007] and 12,550 km^2 [*Skvarca et al.*, 2010], respectively, forming the largest temperate ice mass in the Southern Hemisphere [*Warren and Sugden*, 1993]. Recent studies report that both icefields have been losing ice volume over decadal and longer time scales, contributing to sea level rise (SLR) [*Glasser et al.*, 2011; *Rignot et al.*, 2003; *Willis et al.*, 2012]. *Rignot et al.* [2003] reported that the volume loss of the icefields was equivalent to a SLR of 0.042 ± 0.002 mm a^{-1} from 1968/1975 to 2000, later increasing to 0.067 ± 0.004 mm a^{-1} in 2000–2012 [*Willis et al.*, 2012].

The SPI extends for 350 km north-south along the southern Andes and the Chile–Argentina border, covering an elevation range from 0 to 3400 m above sea level. The climate of the icefield is dominated by westerly winds from the Pacific Ocean and a steep east-west gradient of precipitation across the mountains [*Garreaud et al.*, 2009; *Masiokas et al.*, 2009]. Because many outlet glaciers in Patagonia terminate by calving either into the ocean (western side) or freshwater lakes (mainly eastern side), calving glaciers greatly influence the SPI ice mass budget [*Rignot et al.*, 2003].

Frontal variations of these calving glaciers have been measured for the period before 1944 [*Davies and Glasser*, 2012; *Glasser et al.*, 2011; *Masiokas et al.*, 2009] and for the period 1944–2005 [e.g., *Aniya et al.*, 1997; *Lopez et al.*, 2010]. In particular, *Aniya et al.*'s [1997] measurements revealed that 65% of the 48 outlet glaciers retreated between 1944/1945 and 1985/1986, losing a total area of 200 km^2. *Lopez et al.*'s [2010] measurements revealed that the front-position displacements of 32 glaciers between 1945 and 2005 ranged from −11.6 to 8.3 km. These studies demonstrate a retreating trend during the twentieth century, but the decadal temporal resolution is not fine enough to investigate the details of rapid glacier changes. Moreover, since 2005, there has been no detailed research on frontal variations in the SPI, despite recent abrupt retreats of some calving glaciers there [*Rivera et al.*, 2012a; *Sakakibara et al.*, 2013]. To understand the details and the driving mechanisms of the recent rapid retreats, higher temporal resolutions are required.

Table 1. Landsat Images Used in This Study

Sensor	Number	Period	Path/Row
Landsat 4 (TM)	5	1989–2007	230/95,96, 231/94,95,96, 232/94,95
Landsat 5 (TM)	356	1984–2009	
Landsat 7 (ETM+)	607	1999–2011	

Several calving glaciers in the SPI have changed rapidly over the last decade. These glaciers include Glaciar Upsala, SPI's third largest calving glacier. Upsala retreated 2.9 km from 2008 to 2011 [*Sakakibara et al.*, 2013], and Glaciar Jorge Montt retreated 308 m a^{-1} in 2008/2009 and 716 m a^{-1} in 2010/2011 [*Rivera et al.*, 2012a]. Such abrupt changes cannot be attributed to climatic forcing alone, which leaves ice dynamics as a likely driver of the rapid retreat.

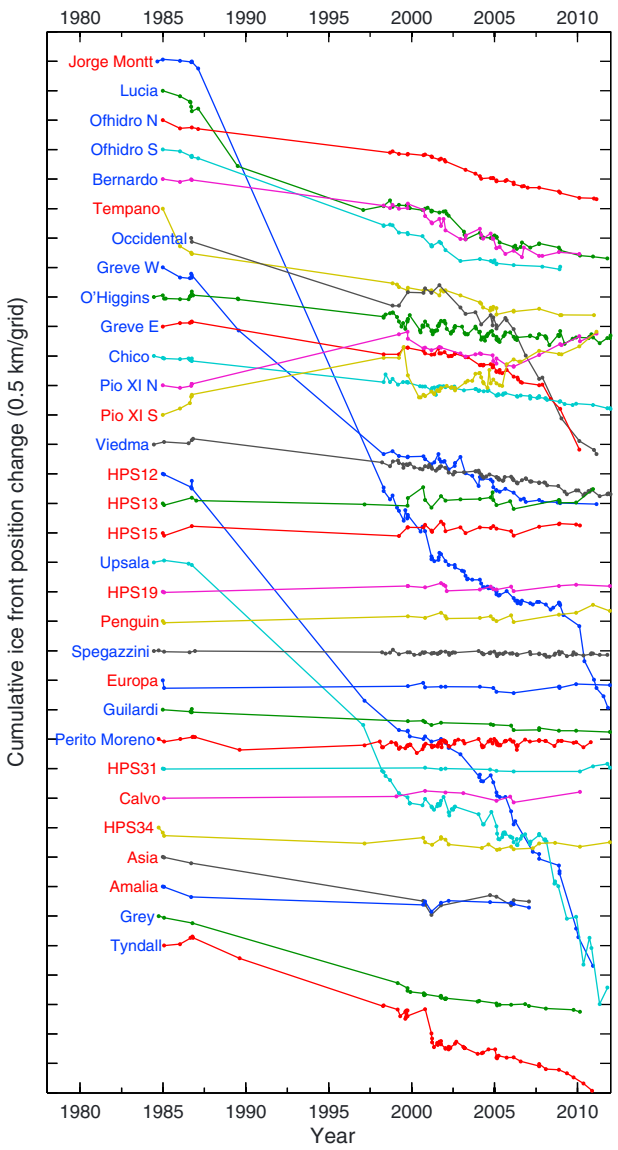

Figure 1. Cumulative changes in the ice-front positions of SPI-calving glaciers from 1984 to 2011. Positive change in the ordinate represents glacial advance. Tidewater-calving glaciers are written in red, while freshwater-calving in blue.

Ice velocity has also been measured on SPI calving glaciers. For example, remote sensing has been used to observe the ice flow on Glaciar Perito Moreno [*Ciappa et al.*, 2010; *Michel and Rignot*, 1999; *Rott et al.*, 1998; *Stuefer et al.*, 2007], Upsala [*Floricioiu et al.*, 2008, 2009; *Sakakibara et al.*, 2013; *Skvarca et al.*, 2003], and Jorge Montt [*Rivera et al.*, 2012b]. Also, in situ ice velocity measurements have been collected from Perito Moreno [*Sugiyama et al.*, 2011], Upsala [*Naruse et al.*, 1995], and Glaciar Pío XI [*Rivera et al.*, 1997]. *Muto and Furuya* [2013] used satellite data to measure the velocity of eight calving glaciers in the SPI from 2002 to 2011. Some glaciers showed significant acceleration accompanied by rapid ice-front retreat. These studies indicate the importance of ice dynamics in the abrupt glacier changes, but spatial and temporal patterns of ice speed in the SPI have been reported only for limited areas and a relatively short time period. The resulting lack of data obscures the role of ice dynamics in the rapid glacier changes in the Patagonian icefields.

Here we present a detailed data set of recent changes in glacier length and ice speed of calving glaciers in the SPI. We analyzed satellite images to measure the frontal positions and ice speeds of 31 termini of 28 calving glaciers (three glaciers have 2 termini). All glaciers have a surface area exceeding 100 km^2, as determined in *Aniya et al.* [1996]. The measurements cover 1984 to 2011 with seasonal-to-decadal resolution. Based on the study results, we discuss the cause of recent glacier changes in the SPI, particularly the importance of ice speed changes in the rapid retreat of calving glaciers.

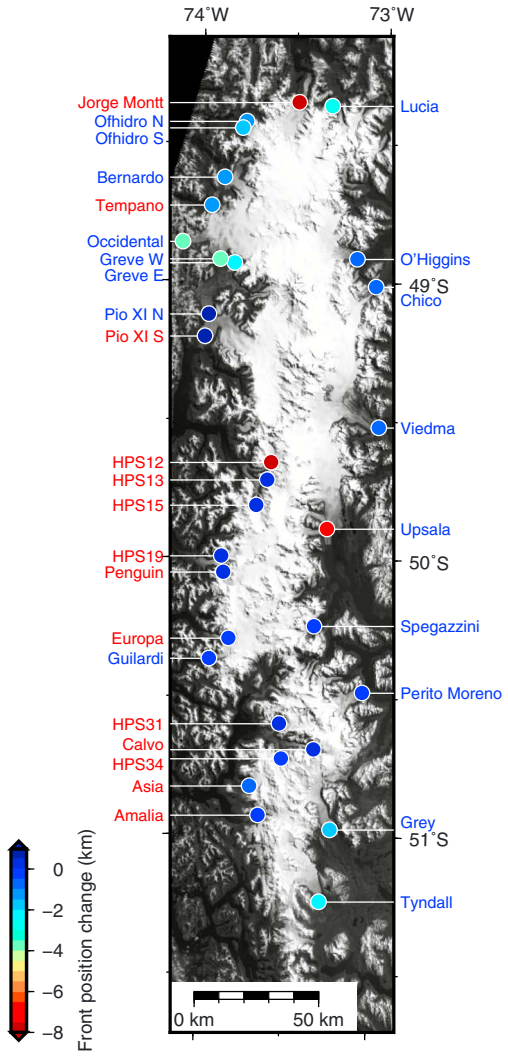

Figure 2. Changes in the glacial front positions from 1984 to 2011 (advance is positive). Tidewater-calving glaciers are written in red, while freshwater calving in blue. Background is a mosaic Landsat 7 ETM+ image acquired in 2001. The white color indicates snow, ice, or cloud-covered regions.

2. Data and Methods

We used satellite images of the Landsat 7 Enhanced Thematic Mapper Plus (ETM+), level 1 T, with 15 m resolution, and used the Landsat 4 and 5 Thematic Mapper (TM), level 1 T, with 30 m resolution distributed by the United States Geological Survey (Table 1). For ETM+ data after 31 May 2003, failure of the scan-line corrector (SLC) resulted in null strips; however, the geometric quality of the data, when properly masked, is as good as the pre-SLC failure data [*Howat et al.*, 2010]. The unavailability of some images limits our observational record to the years 1984–1986 and 1999–2011.

2.1. Glacier Front Position

We used ETM+ and TM images from 1984 to 2011 to map the glaciers' front positions. In each image, the glacier calving front was manually delineated using the ESRI ArcMap geographic information system software. The mean retreat distance was obtained by dividing the areal change between two successive images by the width of the calving front [*Moon and Joughin*, 2008]. The main sources of uncertainty in this measurement are the errors in manual delineation and coregistration of the images. The coregistration error in the repeat Landsat images was ±89 m, based on the horizontal displacement of off-ice surface features. This error was computed by taking one image pixel size as the delineation error [*Paul et al.*, 2013], with the total error estimated as 90 and 93 m for ETM+ and TM images, respectively.

2.2. Ice Speed

We measured ice speeds by calculating the offset of visible surface features between repeat images [*Scambos et al.*, 1992]. The method involved 383 pairs of TM and/or ETM+ images with temporal separations of 16–192 days. To determine the offset, we used the normalized cross correlation of spatial variations in image intensity because this method performs the best on narrow glaciers with good visual contrast [*Heid and Kääb*, 2012], which are the type of glacier studied here. For post-SLC failure images, the offset was calculated using the "null exclusion" scheme developed by *Ahn and Howat* [2011]. To improve the resolution of the speed measurement, we applied bicubic interpolation to a cross-correlation surface on 1/8 pixel size mesh-grid points. This mesh size and the interpolation method are recommended in *Debella-Gilo and Kääb* [2011]. After the computations, all displacement vectors based outside glaciered areas were removed using digital glacier outlines from Global Land Ice Measurements from Space (GLIMS) [*Bishop et al.*, 2004; *Kargel et al.*, 2005; *Raup et al.*, 2007]. The remaining vectors were filtered using a median low-pass filter. Vectors were removed if they deviated by more than 30° or 150 m a^{-1} from a median vector that was computed within either the 5×5 or 3×3 grid areas [*Heid and Kääb*, 2012; *Kääb et al.*, 2005]. To eliminate any remaining false vectors, we used the median values of the displacement fields [*Howat et al.*, 2010].

Possible errors in such a feature-tracking method include (1) ambiguities in the cross-correlation peak, (2) coregistration errors, and (3) false correlations [*Howat et al.*, 2010]. Errors caused by (1) and (2) were estimated from the root-mean-square horizontal displacement of off-ice surface areas, where the displacement should

Table 2. Rate of Change in the Frontal Positions (D)[a]

Glacier	1984/1985/1986–2000 (m a^{-1})	2000–2010/2011 (m a^{-1})
Amalia	−15 ± 8	1 ± 26[d]
Asia	−49 ± 8	8 ± 26[d]
Bernardo	−38 ± 8	−74 ± 13
Calvo	8 ± 9[b]	−2 ± 13
Chico	−32 ± 8	−33 ± 13
Europa	−1 ± 8	0 ± 13
Greve E	−34 ± 8	−177 ± 13
Greve W	−214 ± 8	−76 ± 13
Grey	−84 ± 8	−32 ± 13
Guilardi	−12 ± 8	−16 ± 13
HPS12	−296 ± 8	−372 ± 13
HPS13	10 ± 8	7 ± 13
HPS15	6 ± 8	1 ± 13
HPS19	5 ± 8	2 ± 13
HPS31	1 ± 8	1 ± 13
HPS34	−9 ± 8	−7 ± 13
Jorge Montt	−541 ± 8	−240 ± 13
Lucia	−126 ± 8	−79 ± 13
Occidental	−61 ± 9[c]	−268 ± 13
Ofhidro N	−34 ± 8	−74 ± 13
Ofhidro S	−97 ± 8	−100 ± 26[d]
O'Higgins	−36 ± 8	−17 ± 13
Penguin	5 ± 8	16 ± 13
Perito Moreno	−11 ± 8	5 ± 13
Pío XI N	44 ± 8	19 ± 13
Pío XI S	7 ± 8	97 ± 13
Spegazzini	−2 ± 8	−2 ± 13
Tempano	−55 ± 8	−41 ± 13
Tyndall	−80 ± 9[b]	−135 ± 13
Upsala	−270 ± 8	−274 ± 13
Viedma	−30 ± 8	−41 ± 13
Mean	−66 ± 1.5	−61 ± 3

[a]Positive values indicate glacier advance.
[b]Rates between 1985 and 2000.
[c]Rates between 1986 and 2000.
[d]Rates between 2000 and 2005.

be zero. We excluded displacements exceeding twice the pixel size, as they must have been due to a false correlation. The mean displacement vector was then subtracted from the computed ice flow vector to obtain the bias of the image pairs. The error evaluation and bias adjustment were performed for all image pairs used for the ice speed measurement. Errors caused by (3) were minimized by applying the filters described above. The sum of the errors (1)–(3) computed for each image pair ranges between ±19 and ±300 m a^{-1}, depending on image quality and temporal separation. Gaps in the ice speed data are due to poor coherence between image pairs in snow-covered accumulation areas and in the heavily crevassed terminus region.

The above speed data agree with field data obtained using the Global Positioning System (GPS) for Perito Moreno and with a previous satellite study for Upsala. In particular, for 26 February 2010 to 2 March 2011, *Sugiyama et al.* [2011] measured a GPS ice speed 4.7 km from the front of Perito Moreno at 1.43 m d^{-1}, whereas our remote sensing method gives 1.3 ± 0.14 m d^{-1} for 16 May to 19 July 2010 and 1.4 ± 0.19 m d^{-1} for 27 February to 24 April 2005. Also, near the calving front of Upsala, *Floricioiu et al.* [2008] found (using feature tracking with synthetic aperture radar) a speed of 7 m d^{-1} in October 2008. In good agreement, we find at 6 km from the calving front a speed of 6.6 m d^{-1} in August 2008.

3. Results

3.1. Glacier Front Position

Among the 31 ice fronts studied, only the two termini of Pío XI advanced between 1984 and 2011. Of the other 29, 12 changed less than ±0.5 km and 17 retreated by more than 0.5 km (Figure 1). The results show a large variation

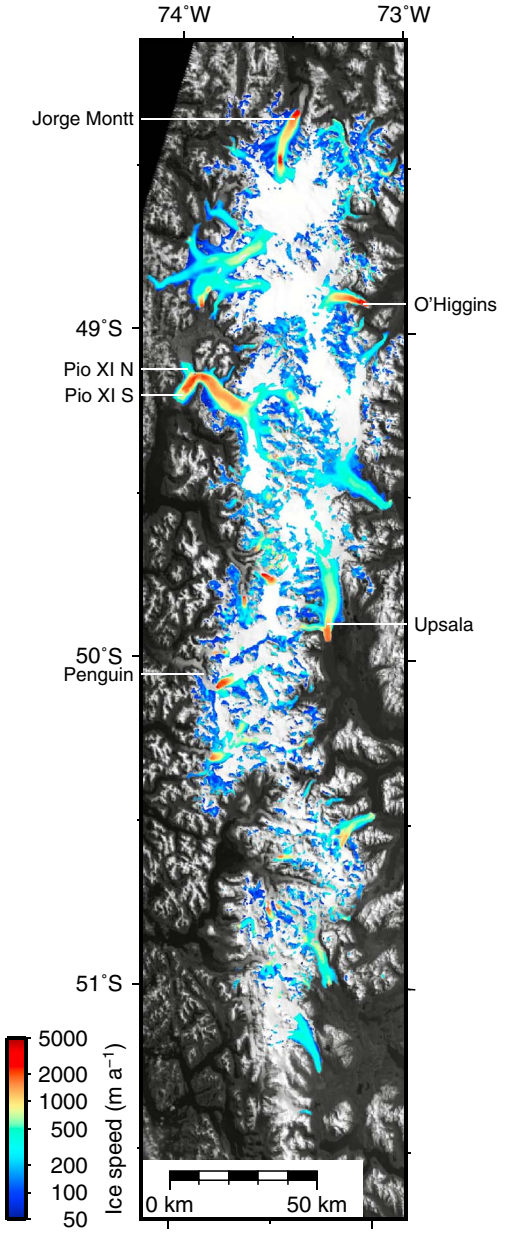

Figure 3. Ice speed distributions over the SPI in 2000–2011. Background is a mosaic Landsat 7 ETM+ image acquired in 2001. The speed at each location equals the mean of all measurements available within the period.

in the magnitude of the retreat (Figure 2). Glaciar Jorge Montt, HPS12, and Upsala retreated over 6 km, which significantly exceeds the mean and median retreat distances of 1.56 km and 0.71 km for all fronts.

Consider the rate of change (m a^{-1}) of the front positions (D) before and after 2000. Between 1984–1986 and 2000, only the northern terminus of Pío XI advanced, while 13 fronts changed little ($|D| < 20$ m a^{-1}) and 17 fronts substantially retreated ($D < -20$ m a^{-1}) (Table 2). Glaciar Jorge Montt, Greve's western terminus, HPS12, and Upsala rapidly retreated with rates exceeding 200 m a^{-1}. Later, between 2000 and 2010/2011, only Pío XI's southern terminus advanced, while 13 fronts showed only small changes ($|D| < 20$ m a^{-1}) and 15 fronts retreated ($D < -20$ m a^{-1}). Glaciar Jorge Montt, Occidental, HPS12, and Upsala retreated at rates exceeding 200 m a^{-1}. Overall, the mean retreat rates were similar during the two periods.

Jorge Montt, HPS12, Upsala, and Pío XI showed significantly greater and more complex frontal variations than the other glaciers (Figure 1). Although Jorge Montt varied only slightly before 1987, it rapidly retreated from 1987 to 1999 at a rate of 620 m a^{-1}. The retreat gradually slowed down between 1998 and 2010, followed by another rapid retreat starting in 2010. The total retreat distance from 1984 to 2011 was 10.44 km (417 m a^{-1}). The retreat rate of HPS12 was 313 m a^{-1} for 1984–2010 but increased in the last year to 630 m a^{-1}. Upsala retreated at 90 m a^{-1} between May 2000 and January 2008 then suddenly increased to 880 m a^{-1} between January 2008 and May 2011. An even greater rate of retreat (2000 m a^{-1}) occurred between November 2010 and May 2011 [*Sakakibara et al.*, 2013]. Unlike the other glaciers, Pío XI consistently advanced, for a total of 1.07 km from 1984 to 2011, except for short retreat episodes such as the 0.86 km retreat from 1999 to 2000. This glacier also has a second calving front further north, which also advanced but by a smaller amount.

3.2. Ice Speed

Figure 3 shows the distribution of mean ice speed over the SPI obtained from Landsat TM and ETM+ image pairs in 2000–2011. The computed ice speed field covers an area of 5461 km^2, covering about 44% of the SPI, with an overall mean value of 820 m a^{-1}. Within 20 km of the termini, the ice speed ranged between 50 ± 40 and 5900 ± 200 m a^{-1}. In general, ocean-terminating glaciers flow faster than lake-terminating glaciers. Most of the former are on the western side of the ice field (e.g., Glaciar Jorge Montt, Pío XI, and Penguin), with a flow speed often exceeding 2000 m a^{-1}. Lake-terminating glaciers flow at rates between 20 and 2940 m a^{-1}, except for Glaciar Upsala and O'Higgins, which flow at speeds exceeding 3000 m a^{-1} near the calving fronts.

The ice speed change was not uniform over the icefield (Figure 4). Between 1984–1986 and 2000, the ice speed changed by less than ±100 m a^{-1} over 63% of the measured area, whereas changes exceeding

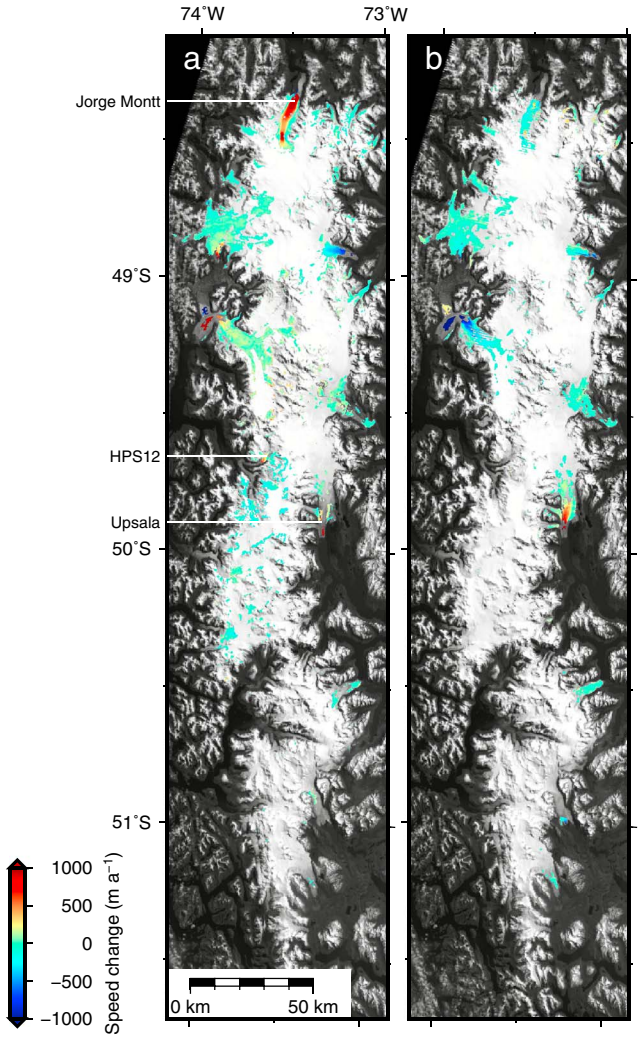

Figure 4. Ice speed changes. (a) Between 1984–1986 and 2000. Background is a mosaic Landsat 7 ETM+ image acquired in 2001. (b) Same as Figure 4a except for between 2000 and 2010/11.

±1000 m a^{-1} occurred over 1.1% of the area. The large ice speed increase occurred in both ocean- and lake-terminating glaciers. The mean ice speed over the studied area increased by 37 m a^{-1} between 1984–1986 and 2000 and decreased by 57 m a^{-1} between 2000 and 2011 (Table 3). The mean speed increase during the first period was primarily due to the large acceleration observed in several glaciers, such as Jorge Montt, HPS12, and Upsala (Table 4). Excluding regions with changes exceeding ±200 m a^{-1}, the mean speed change from 1984 to 2000 was 4 m a^{-1}, and that from 2000 to 2011 was −18 m a^{-1} (−13 m a^{-1} for 1984–2011).

Between 1986 and 2000, ice speeds along the flowline of Jorge Montt increased from 1190 m a^{-1} to 4500 m a^{-1} for ice near the front and increased from 1380 to 2450 m a^{-1} for ice 30 km back from the 1984 calving front (Figure 5a). After the increase, the glacier gradually slowed down until 2004. Then, in 2010, in the area within 25 km of the 1984 front, the ice speed increased by 550–630 m a^{-1} and stayed at this level into 2011.

Between 1986 and 2000, the ice speed at 6 km from the 1985 front of HPS12 increased from 580 to 1400 m a^{-1}, and for ice within 10 km of the front, it increased from 370 to 420 m a^{-1} (Figure 5b). The lowest ~10 km further accelerated in 2007, reaching a maximum speed of ~2800 m a^{-1} near the front.

Near the front of Upsala, the ice speed decelerated from 1870 to 1620 m a^{-1} in 2000–2002, then it accelerated from 1500 to 1850 m a^{-1} in 2004–2007 (Figure 5c). When the glacier started to retreat in 2008, the speed near the front suddenly increased from 1990 to 2400 m a^{-1}, reaching a peak speed of 3400 m a^{-1} at the end of 2010.

In contrast, in the lowest reaches of the southern terminus of Pío XI, the ice speed increased from 2290 to 3980 m a^{-1} between 1986 and 2000, then gradually decreased with small fluctuations, reaching its lowest level in 2008 (Figure 5d).

Table 3. Ice Speed Change Over the Area (Δu)

Period (Year)	Area (km^2)	Speed Change Δu (m a^{-1})	Speed Change Excluding Pixels of $\lvert\Delta u\rvert > \pm 200$ m a^{-1} (m a^{-1})
1984/1985/1986–2010/2011	931	−29.9 ± 0.7	−12.9 ± 0.8
1984/1985/1986–2000	1769	+36.3 ± 0.6	2.1 ± 0.6
2000–2010/2011	1126	−56.8 ± 0.5	−17.8 ± 0.6

Table 4. Relative Changes in the Ice Speed[a]

Glacier	1984/1985/1986–2010/2011 (%)	1984/1985/1986–2000 (%)	2000–2010/2011 (%)
Amalia	NA[c]	NA[c]	8 ± 6[b]
Asia	−16 ± 5[b]	NA[c]	NA[c]
Bernardo	−10 ± 4	−12 ± 4	8 ± 4
Calvo	NA[c]	NA[c]	NA[c]
Chico	−38 ± 4	−21 ± 4	−25 ± 5
Europa	−18 ± 2[b]	−5 ± 2	−11.3 ± 1.7[b]
Greve E	1 ± 4	−14 ± 3	22 ± 3
Greve W	21 ± 3	44 ± 3	−15.3 ± 1.8
Grey	−3 ± 9[b]	27 ± 9	−44 ± 3
Guilardi	−12 ± 15[b]	−10 ± 18	1 ± 11[b]
HPS12	124 ± 12[b]	92 ± 10	19 ± 3[b]
HPS13	2 ± 8	−2 ± 2	5 ± 7
HPS15	−3 ± 7	−1 ± 12	−2 ± 6
HPS19	−9 ± 5	−8 ± 9	10 ± 15
HPS31	−12 ± 7[b]	−5 ± 14	9 ± 13[b]
HPS34	9 ± 3[b]	NA[c]	NA[c]
Jorge Montt	163 ± 3	177 ± 2	4.1 ± 0.6
Lucia	−2 ± 4	−1 ± 3	4 ± 6
Occidental	−2 ± 5	1 ± 3	11 ± 5
Ofhidro N	−6 ± 5	−9 ± 4	2 ± 4
Ofhidro S	−12 ± 4	−7 ± 4	−4 ± 4
O'Higgins	−30.5 ± 0.9	−22.2 ± 0.8	−9.8 ± 1.0
Penguin	−8 ± 4	0.6 ± 1.6	−8 ± 3
Perito Moreno	−7 ± 2	−2.3 ± 1.9	−31 ± 0.9
Pío XI N	−33.1 ± 0.8	−2.9 ± 0.8	−3 ± 3
Pío XI S	−41.4 ± 0.7	34.5 ± 0.7	−57.5 ± 0.4
Spegazzini	NA[c]	NA[c]	20 ± 40
Tempano	−13.6 ± 1.9	−8.5 ± 1.9	−7.4 ± 1.7
Tyndall	−11 ± 7	−20 ± 11	−7 ± 5
Upsala	310 ± 60	120 ± 20	66 ± 2
Viedma	−4 ± 2	3 ± 3	−5.3 ± 1.4
Mean	12 ± 2	13.4 ± 1.5	−0.5 ± 1.8

[a]Each value represents the mean changes along the centerline, within 20 km of the front. Positive values indicate acceleration.
[b]Changes between 1984/1985/1986–2005 and 2000–2005, respectively.
[c]NA indicates no data available.

4. Discussion

4.1. General Trends in Frontal Variations and Ice Speed

Most of the calving glaciers in the SPI have been retreating over the last 27 years (Figure 1), in agreement with aerial changes recently reported by *Davies and Glasser* [2012]. *Aniya et al.* [1997] reported that 65% of the SPI glaciers had lost ice-covered area from 1944/1945 to 1985/1986. Thus, our results indicate that the retreating trend has continued for more than 60 years.

However, some glaciers had a frontal variation pattern that significantly changed after 1986. For instance, the retreat rate of O'Higgins was the greatest in Patagonia for the period 1944–1986, but this glacier retreated at a rate of only 36 m a^{-1} from 1986 to 2000. Similarly, Glaciar Amalia retreated at a rate of 278 m a^{-1} in 1945/1945–1985/1986 [*Aniya et al.*, 1997], whereas the retreat rate from 1986 to 2000 was only 15 m a^{-1}. Compared to these two glaciers, Jorge Montt and Upsala retreated faster during our study period. These observations demonstrate that the glaciers in the SPI have been retreating in general, but their rates are spatially and temporally nonuniform.

Changes in the frontal positions are associated with the observed ice speed variations near the terminus. Figure 6 compares the magnitude of the frontal variation at each glacier and relative ice speed change. Figure 6a illustrates a clear relationship between frontal retreat and glacier acceleration. However, this trend arises from the outliers, the three glaciers with the largest retreat. If we exclude these rapidly changing glaciers, the remaining calving glaciers in the SPI are generally decelerating over the study period (Table 3 and Figure 6b). Although glaciers that retreat less than 0.5 km have little change in relative speed (i.e., below

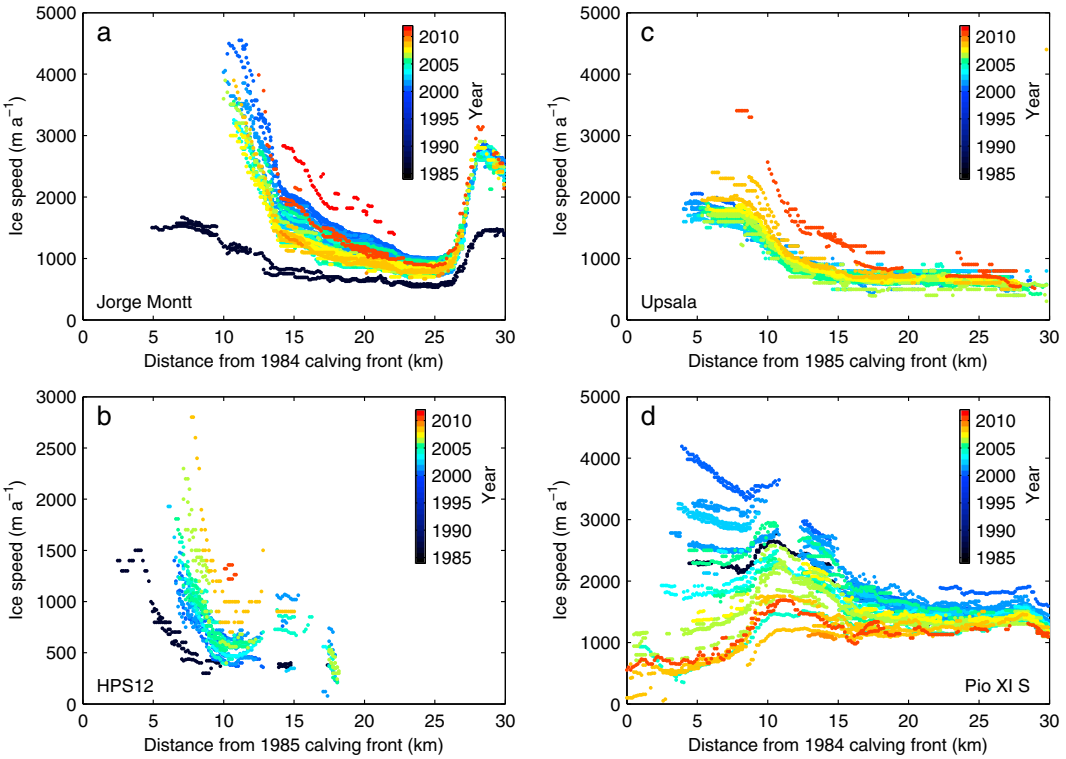

Figure 5. Ice speed along the flowline and its temporal variations at (a) Jorge Montt, (b) HPS12, (c) Upsala, and (d) the southern terminus of Pío XI. (See Figure S1 in the supporting information for similar plots for all other glaciers.)

15%), glaciers that retreat more than 0.5 km show a decrease in speed (Figure 6b and Table 4). Most of the freshwater calving glaciers fall into this latter category, thus largely driving the generally decelerating trend in the SPI.

4.2. Role of the Climate in the SPI Glacier Retreat

A likely driver of the retreat trend lasting for more than 60 years is the warming climate as suggested by *Rignot et al.* [2003]. According to meteorological stations south of 46°S, the climate here has warmed 0.4–1.4° C since the beginning of the last century [*Rosenblüth et al.*, 1995]. This warming trend increases in higher latitudes, especially in the eastern side of the Andes. *Ibarzabal y Donangelo et al.* [1996] found a warming by 0.3°C in the period 1940–1990 at the weather station in El Calafate (50°30′S). Reanalysis data at 50°S 75°W also show a warming of 0.5°C at 850 hPa between 1960 and 1999 [*Rasmussen et al.*, 2007]. As a result of this 0.5°C warming, the melt rate in the ablation areas of the Patagonia icefields has increased an estimated 0.5 m water equivalent [*Rasmussen et al.*, 2007].

The mass balance of Patagonian glaciers is characterized by an extraordinary amount of snowfall in the accumulation area [e.g., *Schwikowski et al.*, 2013; *Shiraiwa et al.*, 2002]. Although data from meteorological stations between 51 and 53°S indicate little variation from 1950 to 2000 [*Aravena and Luckman*, 2009], reanalysis data in the Patagonian icefields show that solid precipitation has decreased about 5% from 1960 to 1999 [*Rasmussen et al.*, 2007]. This decrease can be explained by a shift of some precipitation from snow to rain under the rising temperatures. Such an influence of warming on precipitation may play an important role in the future mass balance of Patagonian icefields, as suggested by a recent modeling study [*Schaefer et al.*, 2013]. Lacking any significant change in accumulation here, the long-term retreat trend is most likely due to an increase in melting arising from the warming climate.

4.3. Acceleration Associated With Rapid Glacier Retreat

In most cases, the observed warming trend can explain the retreat of the glaciers of the SPI. However, the exceptionally rapid retreat of Jorge Montt, HPS12, and Upsala requires additional interpretation. Their retreat

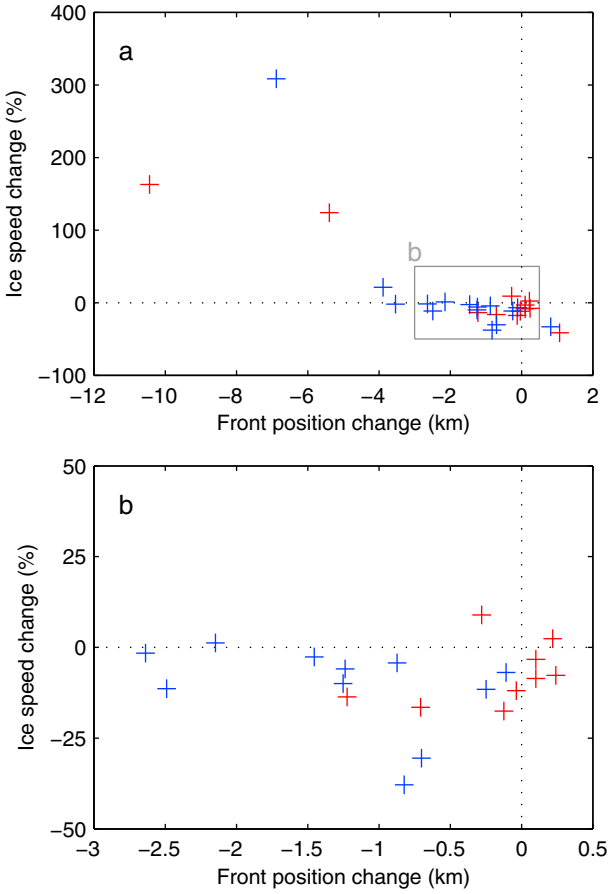

Figure 6. Front position change versus ice speed change. (a) All glaciers from 1984–1986 to 2010/2011. (b) Details of the section indicated by the box in Figure 6a. The Color scheme is the same as that in Figure 1. The speed changes are 20 km averages from Table 4.

rates exceeded 200 m a^{-1} and sometimes reached 500 m a^{-1}. As the rapid retreats of these three glaciers may be driven by ice speed changes, we examine their ice speed changes.

We focus on recent ice speed changes of the rapid-retreating glaciers at two locations on the flowline and compare to the advancing cases (Figure 7). These plots demonstrate close connections between rapid retreat and ice flow acceleration. At 14 km from the front of Jorge Montt, the speed decreased from 2250 to 1510 m a^{-1} between 2000 and 2003 (Figures 7a and 8b). After this deceleration, the speed stayed constant until it sharply increased from 1430 to 2150 m a^{-1} in 2010 (Figure 8c). This acceleration coincides with a rapid terminus retreat. Similar decadal and seasonal speed changes are also observed 20 km from the front. In addition to these decadal-scale speed changes, clear seasonal variations are observed between 2003 and 2007. Maximum and minimum speeds occurred in early and late summer, and the magnitude of the seasonal variations was about 500 m a^{-1}. For other periods, we do not have enough data to analyze the seasonal changes.

At HPS12, the ice speed 8 km from the 1984 front was 940 m a^{-1} in 2000 (Figures 7b and 8e). This speed gradually increased until 2005 with fluctuations, but stayed within 750–1160 m a^{-1}. Then, the glacier further accelerated, reaching a speed of 2600 m a^{-1} in 2008 (Figure 8f). The glacier progressively retreated from 2001 to 2008 at a nearly constant rate, followed by a rapid retreat that began in 2008. In contrast to the speed variations observed near the front, the speed at 12 km from the front was insensitive to the frontal variations.

At 8 km from the 1984 front of Upsala, the ice speed was 1830 m a^{-1} in 2000, decreasing to 1600 m a^{-1} until 2002 (Figure 7c). Then, the glacier gradually accelerated from 2002 to 2008 (Figure 8h), followed by a rapid acceleration from 1970 m a^{-1} to 3400 m a^{-1} over the next 2 years (Figure 8i). This acceleration in 2008 coincides with the onset of a rapid retreat. The speed variation upglacier (14 km from the 1984 front) was similar but of smaller magnitude.

These observations strongly suggest important roles of glacier dynamics in the abrupt changes of the three calving glaciers. The rapid retreats were often accompanied by acceleration, and the timing of acceleration closely agrees with the rapid retreat, particularly at Jorge Montt in 2010 and at Upsala in 2008 (Figures 7a and 7c). The magnitude of the speedup was greater near the front, increasing the stretching flow regime in the lower reaches (Figures 5a and 5c).

In Greenland, a similar acceleration of flow also occurred with rapidly retreating calving glaciers. There, the rapid retreats are associated with accelerations and increasing longitudinal tensile strain rates in the lower reaches, which are thought to result from a reduction in the resistive stress occurring at each terminus [*Howat et al.*, 2007]. Such changes in the stress regime are caused by ice detachment from both the bed and the fjord walls after thinning and by the front retreat. For example, Greenland's Helheim Glacier retreated by 2.1 km from 2001

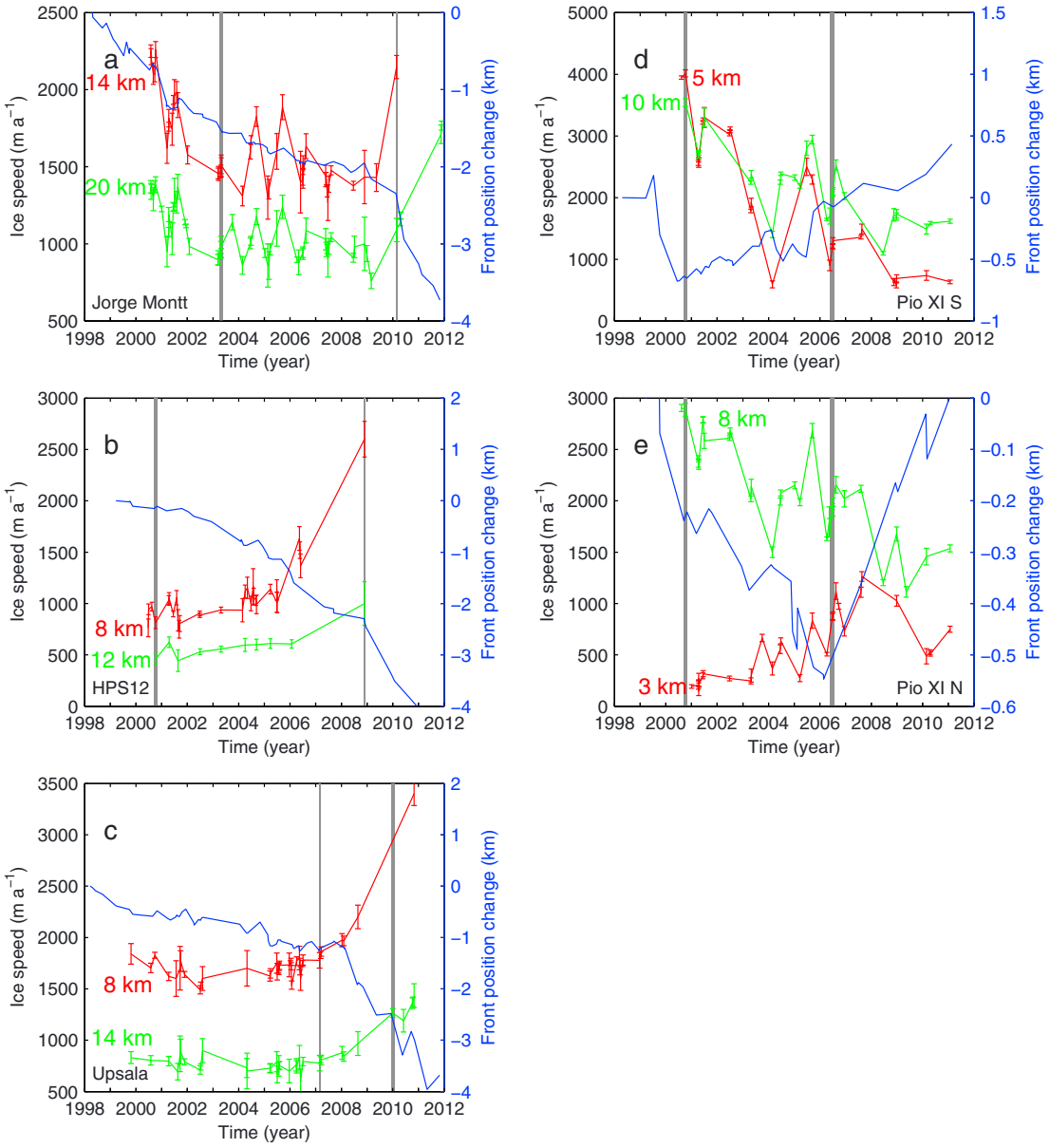

Figure 7. Ice speed and front position for selected glaciers. (a) Ice speeds at 14 and 20 km from the front of Jorge Montt. (b) At 8 and 12 km from the front of HPS12. (c) At 8 and 14 km from the front of Upsala. (d) At 5 and 10 km from the southern front of Pío XI. (e) At 3 and 8 km from the northern front of Pío XI. The distance from the glacier fronts to the sampling sites was measured along the centerline (see Figure 8 for locations). The right axes show the displacements of the front positions since 1998/1999 (in blue). The gray vertical lines indicate the measurement period of the ice speed shown in Figure 8. (See Figure S2 in the supporting information for similar plots for all other glaciers.)

to 2002, which increased by 20% the mean effective driving stress within 12.5 km of the front [*Howat et al.*, 2005]. This increase in stress was proposed as the driving process of the simultaneous 45–60% ice speed increase. The calving flux increases when a glacier accelerates, which leads to thinning and subsequent retreat [*Howat et al.*, 2005; *Joughin et al.*, 2004]. Moreover, thinning near the terminus steepens the ice surface, which causes further acceleration there, as well as acceleration upglacier. We argue that the same type of dynamically controlled glacier retreat also occurred at SPI with the three most rapidly retreating glaciers.

In 2008, Upsala suddenly went from a relatively stable phase to a rapidly retreating, fast-flowing phase. The transition cannot be due to a climatic forcing because no noticeable change was observed in air temperature at a nearby weather station [*Sakakibara et al.*, 2013]. According to previous studies of this glacier, the spatial pattern of bedrock topography controls the changes in its retreat rate and ice speed [*Naruse and Skvarca*, 2000;

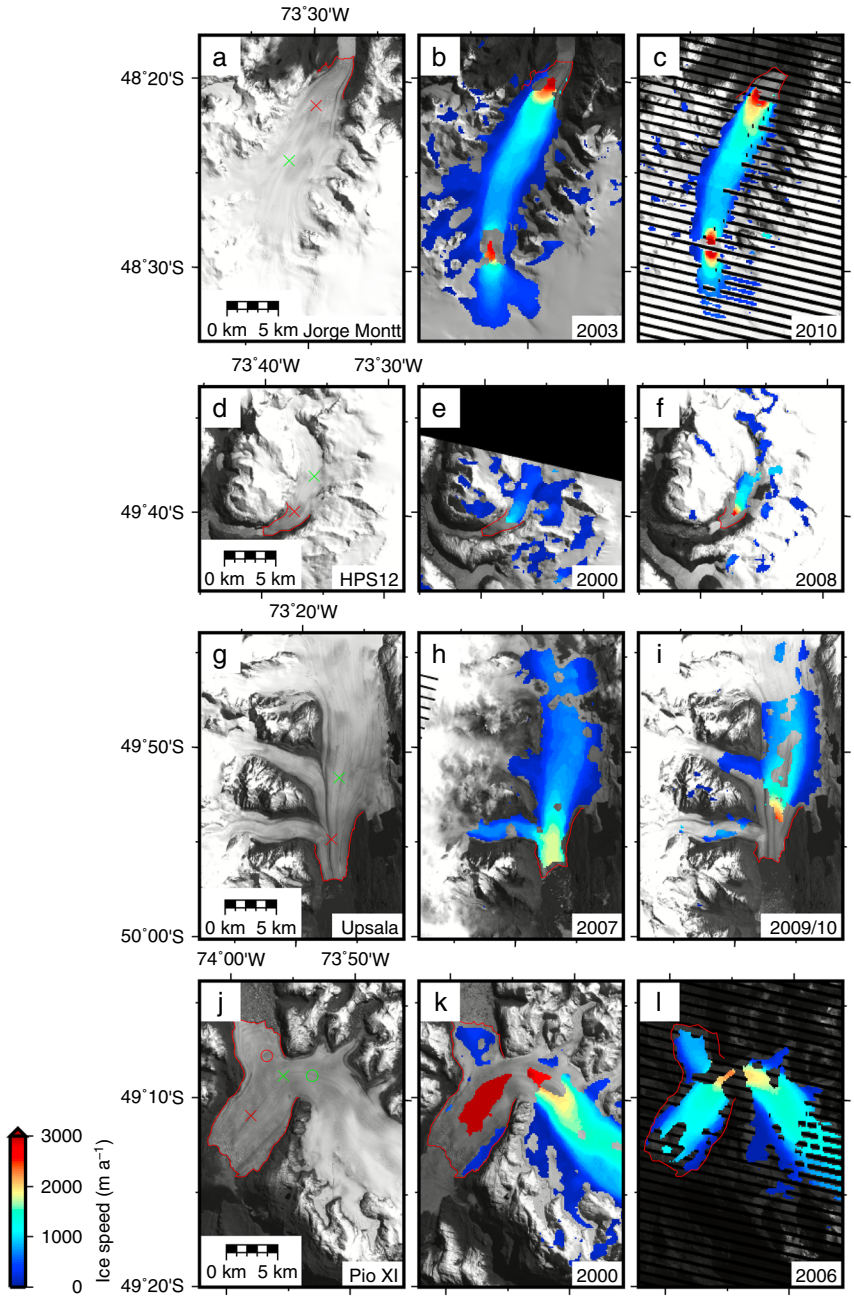

Figure 8. (a) Satellite image of Jorge Montt and ice speed distributions for the periods (b) 2 April to 13 May 2003 and (c) 16 February to 4 March 2010. (d) Image of HPS12 and ice speed for (e) 16 September 2000 to 27 October 2000 and (f) 17 November to 3 December 2008. (g) Image of Upsala and ice speed for (h) 17 February to 5 March 2007 and (i) 7 December 2009 to 24 January 2010. (j) Image of Pío XI and ice speed for (k) 16 September to 27 October 2000 and (l) 28 May to 31 July 2006. The red and green crosses in Figures 8a, 8d, 8g, and 8j indicate lower and upper sampling sites of ice speed data shown in Figures 7a– 7. The red and green circles in Figure 8j mark the two sites shown in Figure 7e. The red lines are partial outlines of each glacier. The images in Figures 8a, 8d, 8g, and 8j were acquired by Landsat 7 ETM+ on 14 October 2001. Each background of Figures 8b, 8c, 8e, 8f, 8h, 8i, 8k, and 8l is a Landsat 7 ETM+ or Landsat 5 TM image acquired on each former date of measurement period.

Skvarca et al., 2002]. Numerical modeling of calving glaciers shows that a transition takes place when the front retreats over a bedrock rise into deeper water [*Nick et al.*, 2009; *Vieli et al.*, 2002]. The rapid retreat and ice speed increase of Jorge Montt after 2010 were also attributed to the seabed geometry [*Rivera et al.*, 2012a]. Thus, it is suggested that the underlying glacier bed topography plays a key role in the rapid changes of both freshwater and tidewater calving glaciers in the SPI.

The geometrically controlled rapid glacier changes are similar to those observed during the retreat phase of the tidewater glacier cycle, originally proposed for Alaskan glaciers [*Meier and Post*, 1987; *Post et al.*, 2011]. This cycle consists of a long, relatively stable phase, then a short period of large retreat and dynamic instability [*Meier and Post*, 1987]. Jorge Montt and Upsala likely went into such a retreating phase in the 1980s, superimposed on a longer-term retreating pattern initially driven by climate change.

Between 2000 and 2012, rapid thinning at rates exceeding 20 m a^{-1} were observed in Jorge Montt, HPS12, and Upsala [*Willis et al.*, 2012]. These rates significantly exceed the SPI mean thinning rate of 1.8 ± 0.1 m a^{-1} [*Willis et al.*, 2012]. During the same period, these three glaciers accelerated in the terminus areas where large thinning rates were reported. Such a speedup near the terminus should have increased the stretching ice flow. For example, near the calving front of Upsala, the longitudinal tensile strain rate increased by 80% after the rapid retreat in 2008 [*Sakakibara et al.*, 2013]. Presumably, dynamical thinning associated with flow acceleration plays an important role in the mass loss of the SPI. The ice mass loss from Upsala from 2000 to 2012 corresponds to 15% of the total loss from the SPI [*Willis et al.*, 2012]. Given that flow acceleration is the primary driver of the rapid retreat of these glaciers, the increase in their ice discharge must account for much of the ice mass loss of the SPI over the last several decades.

4.4. Advance of Glaciar Pío XI

Pío XI, the largest glacier in South America, is the only glacier that advanced during the studied period. Its southern terminus began advancing in 2000, its northern terminus in 2006 (Figure 1, Figures 7d and 7e, and Figures 8k and 8l). According to *Rivera et al.* [1997], this glacier advanced 4 times during the twentieth century (1926–1928, 1945–1951, 1976–1981, and 1992–1994).

The ice speed of both branches of Pío XI showed large, complex variations. In the southern branch, the glacier rapidly slowed down between 2000 and 2004, as shown by the deceleration from 4010 to 590 m a^{-1} at 5 km from the front (Figures 7d and 8k). The speed increased to 2500 m a^{-1} in 2005 but later decreased again to 630 m a^{-1} by the end of 2008 (Figure 8l). The southern terminus progressively advanced during these periods.

The northern branch's ice speed changes were different (Figure 7e). During the retreat of the northern terminus before 2006, the ice speed increased 3 km from the front but decreased 8 km from the front, as observed in the southern terminus (Figure 7d). Presumably, the speed in the upper reaches was influenced by the dynamics of the southern branch, as the sampling site is close to the confluence area (Figure 8j). After the glacier began to advance in 2006, the speed decreased at both locations. Seasonal speed variations were recognized in the northern branch, where the annual peak speed occurs in early summer.

Rivera et al. [1997] suggested that an advance of Pío XI is the glacier's response to a positive precipitation anomaly. That is, the front position is controlled by decadal variations in snowfall over a large accumulation area with a delay time of 10–25 years. The complex frontal and ice speed variations of Pío XI are probably due to mass balance fluctuations in its large accumulation area and also to complex glacier geometry and bed conditions near the calving fronts.

5. Conclusions

We used Landsat satellite images from 1984 to 2011 to measure the frontal positions and ice speeds of 28 calving glaciers in the SPI. The results were used to analyze their frontal variations and to generate ice speed maps covering approximately half of the entire ice field.

Among all 28 glaciers, 1 advanced, 12 were stable (±0.5 km), and 17 retreated by more than 0.5 km over the study period. On average, the glaciers retreated by 1.56 km from the mid-1980s to 2000, and this trend continued until 2011. Three glaciers (Jorge Montt, HPS12, and Upsala) have shown extraordinary large retreat (>6 km) from 1984 to 2011. Near the calving front, the ice speed varied between 50 and 5900 m a^{-1}, and the speed generally decreased over the second half of the study period. Excluding regions with a speed change exceeding ±200 m a^{-1}, the mean speed over the measured area slightly increased (4 m a^{-1}) from 1984 to 2000 and then decreased (-18 m a^{-1}) from 2000 to 2011.

Except for Pío XI, the glaciers fall into one of three categories: stable front position without significant ice speed change, gradual retreat with deceleration, and rapid retreat with large acceleration. The overall retreat

trend was probably due to the long-term warming trend. Nevertheless, our data demonstrated that the extraordinary large retreats in the three glaciers were not directly controlled by the warming trend but instead driven by glacier dynamics. Such dynamically controlled rapid recession of several calving glaciers plays a key role in the recent volume decrease of the SPI.

Acknowledgments

Landsat images were downloaded from http://earthexplorer.usgs.gov. Glacier outlines were downloaded from the GLIMS database http://glims.colorado.edu/glacierdata/. The quality of the manuscript was improved by comments from Pedro Skvarca, Hernán De Angelis, and two anonymous reviewers. We thank Bryn Hubbard for handling the paper as the scientific editor. This research was funded by JSPS KAKENHI grant number 23403006 (2011–2014) and Global COE Program (Establishment of Center for Integrated Field Environmental Science).

References

Ahn, Y., and I. M. Howat (2011), Efficient automated glacier surface ice speed measurement from repeat images using multi-image/multichip and null exclusion feature tracking, *IEEE Trans. Geosci. Remote Sens.*, *49*(8), 2838–2846, doi:10.1109/TGRS.2011.2114891.

Aniya, M., H. Sato, R. Naruse, P. Skvarca, and G. Casassa (1996), The use of satellite and airborne imagery to inventory outlet glaciers of the Southern Patagonia Icefield, South America, *Photogramm. Eng. Remote Sens.*, *62*(12), 1361–1369.

Aniya, M., H. Sato, R. Naruse, P. Skvarca, and G. Casassa (1997), Recent glacier variations in the Southern Patagonia Icefield, South America, *Arct. Alp. Res.*, *29*(1), 1–12.

Aravena, J. C., and B. H. Luckman (2009), Spatio-temporal rainfall patterns in Southern South America, *Int. J. Climatol.*, *29*, 2106–2120.

Bishop, M. P., et al. (2004), Global Land Ice Measurements from Space (GLIMS): Remote sensing and GIS investigations of the Earth's cryosphere, *Geocarto Int.*, *19*(2), 57–84, doi:10.1080/10106040408542307.

Ciappa, A., L. Pietranera, and F. Battazza (2010), Perito Moreno Glacier (Argentina) flow estimation by COSMO SkyMed sequence of high-resolution SAR-X imagery, *Remote Sens. Environ.*, *114*, 2088–2096.

Davies, B. J., and N. F. Glasser (2012), Accelerating shrinkage of Patagonian glaciers from the Little Ice Age (~AD 1870) to 2011, *J. Glaciol.*, *58*(212), 1063–1084, doi:10.3189/2012JoG12J026.

Debella-Gilo, M., and A. Kääb (2011), Sub-pixel precision algorithms for normalized cross-correlation based image matching of mass movements, *Remote Sens. Environ.*, *115*, 130–142.

Floricioiu, D., M. Eineder, H. Rott, and T. Nagler (2008), Velocities of major outlet glaciers of the Patagonia Icefield observed by TerraSAR-X, *Proceedings of '2008 IEEE International Geoscience and Remote Sensing Symposium'*, Boston.

Floricioiu, D., M. Eineder, H. Rott, N. Yague-Martinez, and T. Nagler (2009), Surface velocity and variations of outlet glaciers of the Patagonia Icefields by means of TerraSAR-X, *Proceedings of '2009 IEEE International Geoscience and Remote Sensing Symposium'*, Cape Town, South Africa.

Garreaud, R. D., M. Vuille, R. Compagnucci, and J. Marengo (2009), Present-day South American climate, *Palaeogeogr. Palaeoclimatol. Palaeoecol.*, *281*(3–4), 180–195, doi:10.1016/j.palaeo.2007.10.032.

Glasser, N. F., S. Harrison, K. N. Jansson, K. Anderson, and A. Cowley (2011), Global sea-level contribution from the Patagonian Icefields since the Little Ice Age maximum, *Nat. Geosci.*, *4*(5), 303–307, doi:10.1038/ngeo1122.

Heid, T., and A. Kääb (2012), Evaluation of existing image matching methods for deriving glacier surface displacements globally from optical satellite imagery, *Remote Sens. Environ.*, *118*, 339–355, doi:10.1016/j.rse.2011.11.024.

Howat, I. M., I. Joughin, S. Tulaczyk, and S. Gogineni (2005), Rapid retreat and acceleration of Helheim Glacier, East Greenland, *Geophys. Res. Lett.*, *32*, L22502, doi:10.1029/2005GL024737.

Howat, I. M., I. Joughin, and T. A. Scambos (2007), Rapid changes in ice discharge from Greenland outlet glaciers, *Science*, *315*(5818), 1559–1561, doi:10.1126/science.1138478.

Howat, I. M., J. E. Box, Y. Ahn, A. Herrington, and E. M. McFadden (2010), Seasonal variability in the dynamics of marine terminating outlet glaciers in Greenland, *J. Glaciol.*, *56*(198), 601–613, doi:10.3189/002214310793146232.

Ibarzabal y Donangelo, T., J. Hoffmann, and R. Naruse (1996), Recent climate changes in Southern Patagonia, *Bull. Glacier Res.*, *14*, 29–36.

Joughin, I., W. Abdalati, and M. Fahnestock (2004), Large fluctuations in speed on Greenland's Jakobshavn Isbræ glacier, *Nature*, *432*(7017), 608–610, doi:10.1038/nature03130.

Kääb, A., B. Lefauconnier, and K. Melvold (2005), Flow field of Krönebreen, Svalbard, using repeated Landsat 7 and ASTER data, *Ann. Glaciol.*, *42*, 7–13.

Kargel, J. S., et al. (2005), Multispectral imaging contributions to global land ice measurements from space, *Remote Sens. Environ.*, *99*, 187–219, doi:10.1016/j.rse.2005.07.004.

Lopez, P., P. Chevallier, V. Favier, B. Pouyaud, F. Ordenes, and J. Oerlemans (2010), A regional view of fluctuations in glacier length in southern South America, *Global Planet. Change*, *71*, 85–108.

Masiokas, M. H., A. Rivera, L. E. Espizua, R. Villalba, S. Delgado, and J. C. Aravena (2009), Glacier fluctuations in extratropical South America during the past 1000 years, *Palaeogeogr. Palaeoclimatol. Palaeoecol.*, *281*, 242–268.

Meier, M. F., and A. Post (1987), Fast tidewater glaciers, *J. Geophys. Res.*, *92*(B9), 9051–9058, doi:10.1029/JB092iB09p09051.

Michel, R., and E. Rignot (1999), Flow of Glaciar Moreno, Argentina, from repeat-pass Shuttle Imaging Radar images: Comparison of the phase correlation method with radar interferometry, *J. Glaciol.*, *45*(149), 93–100.

Moon, T., and I. Joughin (2008), Changes in ice front position on Greenland's outlet glaciers from 1992 to 2007, *J. Geophys. Res.*, *113*, F02022, doi:10.1029/2007JF000927.

Muto, M., and M. Furuya (2013), Surface velocities and ice-front positions of eight major glaciers in the Southern Patagonian Ice Field, South America, from 2002 to 2011, *Remote Sens. Environ.*, *139*, 50–59, doi:10.1016/j.rse.2013.07.034.

Naruse, R., and P. Skvarca (2000), Dynamic features of thinning and retreating Glaciar Upsala, a lacustrine calving glacier in southern Patagonia, *Arct. Antarct. Alp. Res.*, *32*(4), 485–491.

Naruse, R., M. Aniya, P. Skvarca, and G. Casassa (1995), Recent variations of calving glaciers in Patagonia, South America, revealed by ground surveys, satellite-data analyses and numerical experiments, *Ann. Glaciol.*, *21*, 297–303.

Nick, F. M., A. Vieli, I. M. Howat, and I. Joughin (2009), Large scale changes in Greenland outlet glacier dynamics triggered at the terminus, *Nat. Geosci.*, *2*(2), 110–114, doi:10.1038/ngeo394.

Paul, F., et al. (2013), On the accuracy of glacier outlines derived from remote sensing data, *Ann. Glaciol.*, *54*(63), 171–182, doi:10.3189/2013AoG63A296.

Post, A., S. O'Neel, R. J. Motyka, and G. Streveler (2011), A complex relationship between calving glaciers and climate, *Eos Trans. AGU*, *92*(37), 305–306, doi:10.1029/2011EO370001.

Rasmussen, L. A., H. Conway, and C. F. Raymond (2007), Influence of upper air conditions on the Patagonia icefields, *Global Planet. Change*, *59*(1–4), 203–216.

Raup, B., A. Racoviteanu, S. Jodha, S. Khalsa, C. Helm, R. Armstrong, and Y. Arnaud (2007), Remote sensing and GIS technology in the Global Land Ice Measurements from Space (GLIMS) project, *Comput. Geosci.*, *33*, 104–125.

Rignot, E., A. Rivera, and G. Casassa (2003), Contribution of the Patagonia Icefields of South America to sea level rise, *Science*, *302*(6544), 434–437, doi:10.1126/science.1087393.

Rivera, A., H. Lange, J. C. Aravena, and G. Casassa (1997), The 20th century advance of Glaciar Pío XI, Chilean Patagonia, *Ann. Glaciol.*, *24*, 66–71.

Rivera, A., T. Benham, G. Casassa, J. Bamber, and J. Dowdeswell (2007), Ice elevation and areal changes of glaciers from the Northern Patagonia Icefield, Chile, *Global Planet. Change*, *59*, 126–137.

Rivera, A., M. Koppes, C. Bravo, and J. Aravena (2012a), Little ice age advance and retreat of Glaciar Jorge Montt, Chilean Patagonia, *Clim. Past*, *8*, 403–414.

Rivera, A., J. Corripio, C. Bravo, and S. Cisternas (2012b), Glaciar Jorge Montt (Chilean Patagonia) dynamics derived from photos obtained by fixed cameras and satellite image feature tracking, *Ann. Glaciol.*, *53*(60), 147–155.

Rosenblüth, B., G. Casassa, and H. Fuenzalida (1995), Recent climatic changes in western Patagonia, *Bull. Glacier Res.*, *13*, 127–132.

Rott, H., M. Stuefer, A. Siegel, P. Skvarca, and A. Eckstaller (1998), Mass fluxes and dynamics of Moreno Glacier, Southern Patagonia Icefield, *Geophys. Res. Lett.*, *25*(9), 1407–1410, doi:10.1029/98GL00833.

Sakakibara, D., S. Sugiyama, T. Sawagaki, S. Marinsek, and P. Skvarca (2013), Rapid retreat, acceleration, and thinning of Glaciar Upsala in the Southern Patagonia Icefield, initiated in 2008, *Ann. Glaciol.*, *54*(63), 131–138.

Scambos, T. A., M. J. Dutkiewicz, J. C. Wilson, and R. A. Bindschadler (1992), Application of image cross-correlation to the measurement of glacier ice speed using satellite image data, *Remote Sens. Environ.*, *42*, 177–186.

Schaefer, M., H. Machguth, M. Falvey, and G. Casassa (2013), Modeling past and future surface mass balance of the Northern Patagonia Icefield, *J. Geophys. Res. Earth Surf.*, *118*, 571–588, doi:10.1002/jgrf.20038.

Schwikowski, M., M. Schläppi, P. Santibañez, A. Rivera, and G. Casassa (2013), Net accumulation rates derived from ice core stable isotope records of Pío XI glacier, Southern Patagonia Icefield, *Cryosphere*, *7*, 1635–1644.

Shiraiwa, T., S. Kohshima, R. Uemura, N. Yoshida, S. Matoba, J. Uetake, and M. A. Godoi (2002), High net accumulation rates at Campo de Hielo Patagonico Sur, South America, revealed by analysis of a 45.97 m long ice core, *Ann. Glaciol.*, *35*(35), 84–90, doi:10.3189/172756402781816942.

Skvarca, P., H. de Angelis, R. Naruse, C. R. Warren, and M. Aniya (2002), Calving rates in fresh water: New data from southern Patagonia, *Ann. Glaciol.*, *34*, 379–384.

Skvarca, P., B. Raup, and H. de Angelis (2003), Recent behaviour of Glaciar Upsala, a fast-flowing calving glacier in Lago Argentino, southern Patagonia, *Ann. Glaciol.*, *36*, 184–188.

Skvarca, P., S. Marinsek, and M. Aniya (2010), Documenting 23 years of areal loss of Hielo Patagónico Sur, recent climate data and potential impact on Río Santa Cruz water discharge, *Abstract Book of International Glaciological Conference Ice and Climate Change*: *A View from the South*, Valdivia, Chile, Centro de Estudios Cientificos, 82.

Stuefer, M., H. Rott, and P. Skvarca (2007), Glaciar Perito Moreno, Patagonia: Climate sensitivities and glacier characteristics preceding the 2003/04 and 2005/06 damming events, *J. Glaciol.*, *53*(180), 3–16.

Sugiyama, S., P. Skvarca, N. Naito, H. Enomoto, S. Tsutaki, K. Tone, S. Marinsek, and M. Aniya (2011), Ice speed of a calving glacier modulated by small fluctuations in basal water pressure, *Nat. Geosci.*, *4*(9), 597–600, doi:10.1038/ngeo1218.

Vieli, A., J. Jania, and L. Kolondra (2002), The retreat of a tidewater glacier: Observations and model calculations on Hansbreen, Spitsbergen, *J. Glaciol.*, *48*(163), 592–600.

Warren, C. R., and D. E. Sugden (1993), The Patagonian Icefields: A glaciological review, *Arct. Alp. Res.*, *25*(4), 316–331.

Willis, M. J., A. K. Melkonian, M. E. Pritchard, and A. Rivera (2012), Ice loss from the Southern Patagonian Ice Field, South America, between 2000 and 2012, *Geophys. Res. Lett.*, *39*, L17501, doi:10.1029/2012GL053136.